

This discussion paper is/has been under review for the journal Hydrology and Earth System Sciences (HESS). Please refer to the corresponding final paper in HESS if available.

**Part 1: Retrieving
state profiles with
linear and nonlinear
numerical schemes**

G. B. Chirico et al.

Kalman filters for assimilating near-surface observations in the Richards equation – Part 1: Retrieving state profiles with linear and nonlinear numerical schemes

G. B. Chirico¹, H. Medina², and N. Romano¹

¹Department of Agricultural Engineering, University of Naples Federico II, Naples, Italy

²Department of Basic Sciences, Agrarian University of Havana, Havana, Cuba

Received: 3 November 2012 – Accepted: 24 November 2012 – Published: 3 December 2012

Correspondence to: G. B. Chirico (gchirico@unina.it)

Published by Copernicus Publications on behalf of the European Geosciences Union.

Title Page

Abstract

Introduction

Conclusions

References

Tables

Figures

⏪

⏩

◀

▶

Back

Close

Full Screen / Esc

Printer-friendly Version

Interactive Discussion

Abstract

This paper examines the potential of different algorithms, based on the Kalman filtering approach, for assimilating near-surface observations in a one-dimensional Richards' equation. Our specific objectives are: (i) to compare the efficiency of different Kalman filter algorithms, implemented with different numerical schemes of the Richards equation, in retrieving soil water potential profiles; (ii) to evaluate the performance of these algorithms when nonlinearities arise from the nonlinearity of the observation equation, i.e. when surface soil water content observations are assimilated to retrieve pressure head values. The study is based on a synthetic simulation of an evaporation process from a homogeneous soil column. A standard Kalman Filter algorithm is implemented with both an explicit finite difference scheme and a Crank-Nicolson finite difference scheme of the Richards equation. Extended and Unscented Kalman Filters are instead both evaluated to deal with the nonlinearity of a backward Euler finite difference scheme. While an explicit finite difference scheme is computationally too inefficient to be implemented in an operational assimilation scheme, the retrieving algorithm implemented with a Crank-Nicolson scheme is found computationally more feasible and robust than those implemented with the backward Euler scheme. The Unscented Kalman Filter reveals as the most practical approach when one has to deal with further nonlinearities arising from the observation equation, as result of the nonlinearity of the soil water retention function.

1 Introduction

Soil water dynamics in the vadose zone is a critical process that exerts a large control on the water and energy balance of land-atmosphere systems over a wide range of space-time scales (e.g. Milly and Dunne, 1994; Entekhabi et al., 1996; Rodríguez-Iturbe and Porporato, 2005). With the increasing availability of near-surface data from remote and ground-based sensors, unique opportunities emerge to predict the soil

HESSD

9, 13291–13327, 2012

Part 1: Retrieving state profiles with linear and nonlinear numerical schemes

G. B. Chirico et al.

Title Page

Abstract

Introduction

Conclusions

References

Tables

Figures



Back

Close

Full Screen / Esc

Printer-friendly Version

Interactive Discussion



filter (EKF), which relies on the linearization of model using first order approximation of Taylor series, was one of the first, but still widely used, approaches to deal with nonlinear models. Reported drawbacks of the EKF in presence of marked nonlinearities have enhanced further developments as the Ensemble Kalman Filter (Evensen, 2003), based on a statistical replication of the mean state variable using a Monte Carlo technique. Another recent method is the Unscented Kalman Filter (UKF) developed by Julier et al. (1995) and Julier and Uhlmann (1997, 2004), also based on a replication of the mean state variable, but in a deterministic way. Despite the advances in the development of KF, their implementation at large scales is still limited by the high dimensionality of the dynamic systems in the common hydrological applications (Mclaughlin, 2002).

The nonlinearity of the Richards equation during the assimilation of near-surface information can be treated by two alternative approaches: (i) using a Standard Kalman Filter (SKF), thus providing an exact solution of the mean and variance of the state variable, with a linear numerical scheme or (ii) using a non-standard KF, such as EKF or UKF, which supplies an approximate solution of the first two moments of the state variable, but with a nonlinear dynamic state space model. Pondering the advantages and limitations of these two alternative approaches is essential to identify the best strategy for implementing assimilation algorithms in operational soil hydrological studies.

The general aim of this paper is to examine the feasibility of implementing Kalman Filter algorithms to deal with the inherent nonlinearity of the Richards equation. Our first specific objective is to compare the efficiency of soil moisture profile retrieval algorithms involving standard and non-standard Kalman Filter methods as related to different numerical schemes of the h -based form of the Richards equation. A second objective is to evaluate the performance of these retrieval approaches when the further nonlinearities arise from the observation model in the state space dynamic system, as it occurs when surface soil water content values are assimilated to retrieve pressure head profiles with an h -based form of the Richards equation. These analyses are conducted by

Part 1: Retrieving state profiles with linear and nonlinear numerical schemes

G. B. Chirico et al.

Title Page

Abstract

Introduction

Conclusions

References

Tables

Figures



Back

Close

Full Screen / Esc

Printer-friendly Version

Interactive Discussion

repeating the same numerical experiment conducted by Walker et al. (2001), simulating an evaporation process from a homogeneous soil column.

The paper is structured as follows: Sect. 2 illustrates the Kalman Filter algorithms employed in this study; Sect. 3 presents the different numerical schemes of the Richards equation; Sect. 4 describes the results of the numerical experiments; Sect. 5 is devoted to the conclusions.

2 Kalman filtering

The Kalman Filter is a recursive filter that estimates the state of a dynamic system from a series of noise corrupted measurements. Its basic theory, although originally proposed for linear systems (Kalman, 1960), has been implemented into several advanced methods for studying the dynamics of nonlinear systems.

In the most general case, the dynamic system and the measurements are described by two sets of equations, discretised in the time domain (e.g. van der Merwe; 2004):

$$\mathbf{x}_k = F(\mathbf{x}_{k-1}, \mathbf{u}_{k-1}, \mathbf{v}_{k-1}; \mathbf{w}) \quad (1)$$

$$\mathbf{y}_k = H(\mathbf{x}_k, \mathbf{n}_k; \mathbf{w}). \quad (2)$$

F is the dynamic system model which predicts the current hidden system state vector \mathbf{x}_k from the previous state vector \mathbf{x}_{k-1} in response to the current exogenous input vector \mathbf{u}_k , which is assumed known. F is characterized by a vector of time-invariant parameters \mathbf{w} . H is the measurement model, which describes how the current measurements vector \mathbf{y}_k is related to the model parameters \mathbf{w} and the current state \mathbf{x}_k . The dynamic system model is assumed corrupted by a process noise vector \mathbf{v}_{k-1} . Similarly, the measurement model is assumed corrupted by a measurement noise vector \mathbf{n}_k . Both noise vectors are drawn from zero mean multivariate normal distributions, with covariance matrices \mathbf{Q}_k and \mathbf{R}_k , reflecting respectively the uncertainty in the model predictions and measurements.

Part 1: Retrieving state profiles with linear and nonlinear numerical schemes

G. B. Chirico et al.

Title Page

Abstract

Introduction

Conclusions

References

Tables

Figures



Back

Close

Full Screen / Esc

Printer-friendly Version

Interactive Discussion



Part 1: Retrieving state profiles with linear and nonlinear numerical schemes

G. B. Chirico et al.

Title Page

Abstract

Introduction

Conclusions

References

Tables

Figures

◀

▶

◀

▶

Back

Close

Full Screen / Esc

Printer-friendly Version

Interactive Discussion



With respect to the more general Bayesian theory, the system state \mathbf{x}_k evolves over time t_k according to a hidden Markov process, with a conditional probability density $p(\mathbf{x}_k|\mathbf{x}_{k-1})$ fully specified by F and by the process noise distribution $p(\mathbf{v}_{k-1}) \in N(0, \mathbf{Q}_{k-1})$. The observations \mathbf{y}_k are independent from all other states prior to the current state and are generated according to the conditional probability density $p(\mathbf{y}_k|\mathbf{x}_k)$, which is fully specified by H and the observation noise distribution $p(\mathbf{u}_k) \in N(0, \mathbf{R}_k)$.

The Kalman Filter describes the dynamic evolution of the system by providing the first two moments of the state distribution:

- the mean state $\hat{\mathbf{x}}_k = E[\mathbf{x}_k]$, corresponding to the estimated state;
- the covariance of the state distribution $\mathbf{P}_{x_k} = E[(\mathbf{x}_k - \hat{\mathbf{x}}_k)(\mathbf{x}_k - \hat{\mathbf{x}}_k^T)]$, which is equivalent to the error covariance matrix, i.e. a measure of the accuracy of the estimated state.

The two moments are computed according to two different phases: a prediction phase and an update phase. During the prediction phase, an a priori estimate of the state $\hat{\mathbf{x}}_k^- = E[F(\mathbf{x}_{k-1}, \mathbf{u}_{k-1}; \mathbf{w})]$ and its covariance matrix $\mathbf{P}_{x_k}^-$ are provided based on the information available at time step t_{k-1} .

The update phase is activated as the measurements \mathbf{y}_k become available. In this phase, an a posteriori state estimate $\hat{\mathbf{x}}_k$ is provided by a linear combination of the a priori estimate $\hat{\mathbf{x}}_k^-$ and the measurement *innovation*, equal to the difference between the actual measurements \mathbf{y}_k and the a priori prediction of the measurements $\hat{\mathbf{y}}_k^- = E[H(\hat{\mathbf{x}}_k^-; \mathbf{w})]$:

$$\hat{\mathbf{x}}_k = \hat{\mathbf{x}}_k^- + \mathbf{K}_k (\mathbf{y}_k - \hat{\mathbf{y}}_k^-). \quad (3)$$

In Eq. (3), the innovation is weighted through the matrix \mathbf{K}_k , which is chosen as the *gain* minimizing the a posteriori error covariance \mathbf{P}_{x_k} :

$$\mathbf{K}_k = E[(\mathbf{x}_k - \hat{\mathbf{x}}_k^-)(\mathbf{y}_k - \hat{\mathbf{y}}_k^-)^T] E[(\mathbf{y}_k - \hat{\mathbf{y}}_k^-)(\mathbf{y}_k - \hat{\mathbf{y}}_k^-)^T]^{-1} = \mathbf{P}_{x_k} \mathbf{y}_k^- [\mathbf{P}_{y_k}^-]^{-1}. \quad (4)$$

The a posteriori error covariance $\mathbf{P}_{x,k}$ is estimated as follows:

$$\hat{P}_{x_k} = P_{x_k}^- - \mathbf{K}_k P_{y_k}^- \mathbf{K}_k^T \quad (5)$$

In case the dynamic system model and the measurement model are both linear, the covariance matrices $\mathbf{P}_{x_k}^-$ in the prediction phase, and the Kalman *gain* \mathbf{K}_k in the update phase, can be computed by closed linear relations. Moreover, the a posteriori state $\hat{\mathbf{x}}_k$ is the optimal estimate, with the minimum mean square error.

Methods have been designed for applying the Kalman Filter general theory to nonlinear systems. These methods can be grouped in two classes. Methods, such as the Extended Kalman Filter (Gelb, 1974), attempt to propagating the first two moments of the state distribution, through the explicit linearization of the underlying nonlinear model. Other methods, such as the Ensemble (Evensen, 2003) and the Unscented Kalman Filters (Julier et al., 1995; Julier and Uhlmann, 1997, 2004; van der Merwe, 2004), sample the state distribution and propagate it, trying to preserve its first two moments.

2.1 Extended Kalman Filter

Within the general framework of the Kalman Filter, the Extended Kalman Filter (EKF) is undoubtedly the most widely used approach for dealing with nonlinearity. EKF is based on a first order linearization in the Taylor series of the nonlinear operators F and H around the current state.

The a priori estimate of the covariance matrix is calculated as follows:

$$\hat{P}_{x_k}^- = \mathbf{G}_{k-1} \mathbf{P}_{x_{k-1}} \mathbf{G}_{k-1}^T + \mathbf{L}_{k-1} \mathbf{Q}_{k-1} \mathbf{L}_{k-1}^T \quad (6)$$

where \mathbf{G} and \mathbf{L} are respectively the Jacobians matrices of \mathbf{F} with respect to the state vector \mathbf{x} (computed at $\hat{\mathbf{x}}_{k-1}$) and the process noise vector \mathbf{v} (computed at the mean value $\bar{\mathbf{v}} = 0$):

Part 1: Retrieving state profiles with linear and nonlinear numerical schemes

G. B. Chirico et al.

Title Page

Abstract

Introduction

Conclusions

References

Tables

Figures

⏪

⏩

◀

▶

Back

Close

Full Screen / Esc

Printer-friendly Version

Interactive Discussion



$$\mathbf{G}_{k-1} = \left. \frac{\partial F(\mathbf{x}, \mathbf{u}_{k-1}, 0)}{\partial \mathbf{x}} \right|_{\hat{\mathbf{x}}_{k-1}} \quad (7)$$

$$\mathbf{L}_{k-1} = \left. \frac{\partial F(\hat{\mathbf{x}}_{k-1}, \mathbf{u}_{k-1}, \mathbf{v})}{\partial \mathbf{v}} \right|_{\bar{\mathbf{v}}=0} \quad (8)$$

The Kalman gain and the a posteriori estimate of the covariance matrix are computed as follows:

$$\mathbf{K}_k = \mathbf{P}_{x_k}^- \mathbf{C}_k^T (\mathbf{C}_k \mathbf{P}_{x_k}^- \mathbf{C}_k^T + \mathbf{D}_k \mathbf{R}_k \mathbf{D}_k^T)^{-1} \quad (9)$$

$$\mathbf{P}_{x_k} = (\mathbf{I} - \mathbf{K}_k \mathbf{C}_k) \mathbf{P}_{x_k}^- \quad (10)$$

where \mathbf{C} and \mathbf{D} are respectively the Jacobians matrices of H with respect to the state vector \mathbf{x} (computed at the a priori estimate $\hat{\mathbf{x}}_{k-1}^-$) and the observation noise vector \mathbf{n} (at the mean value $\bar{\mathbf{n}} = 0$):

$$\mathbf{C}_k = \left. \frac{\partial H(\mathbf{x}, \mathbf{n}_k)}{\partial \mathbf{x}} \right|_{\hat{\mathbf{x}}_k^-} \quad (11)$$

$$\mathbf{D}_k = \left. \frac{\partial H(\hat{\mathbf{x}}_k^-, \mathbf{n})}{\partial \mathbf{n}} \right|_{\bar{\mathbf{n}}=0} \quad (12)$$

First order continuity of the operator F and H around the current state is required for computing the derivatives presented above. In case the operator F or H are characterized by complex mathematical structures, the derivation of closed expressions for Jacobian matrices may be difficult to obtain in a closed analytical form, thus requiring the implementation of numerical solutions for the derivatives at each update step.

The EKF is subjected to instabilities and even divergence when the approximation to the zero and first order derivatives are not able to capture the correct dynamics of the underlying systems, due to its high nonlinearity.

Part 1: Retrieving state profiles with linear and nonlinear numerical schemes

G. B. Chirico et al.

Title Page

Abstract

Introduction

Conclusions

References

Tables

Figures

⏪

⏩

◀

▶

Back

Close

Full Screen / Esc

Printer-friendly Version

Interactive Discussion



Some KF applications (e.g. Walker et al., 2001) assume that the process noise \mathbf{v} does not propagate through the system model rather it adds directly to the system state:

$$\mathbf{x}_k = F(\mathbf{x}_{k-1}, \mathbf{u}_{k-1}; \mathbf{w}) + \mathbf{v}_{k-1}. \quad (13)$$

In this case, the process noise covariance \mathbf{Q} contributes to the a priori prediction, without being transformed by the Jacobian matrix \mathbf{L} :

$$\hat{\mathbf{P}}_{\mathbf{x}_k}^- = \mathbf{G}_{k-1} \mathbf{P}_{\mathbf{x}_{k-1}} \mathbf{G}_{k-1}^T + \mathbf{Q}_{k-1}. \quad (14)$$

This approach can provide satisfactory results in case the process noise covariance is assumed constant or small as compared with the state covariance; divergence problems may arise otherwise.

2.2 Unscented Kalman Filter

The Unscented Kalman Filter (UKF) belongs to a wider group of approaches known as Sigma Point Kalman Filters (van der Merwe, 2004). The UKF is based on the Unscented Transformation (UT) introduced by Julier and Uhlman (1997, 2004) as an effective method for capturing the nonlinear propagation of the first two moments of the state distribution through a minimal set of deterministically chosen sample points.

The UKF, in its most general structure, is applied to an *augmented* state vector \mathbf{x}_k^a , defined by system state, the process and observation noise vectors:

$$\mathbf{x}_k^a = \begin{bmatrix} \mathbf{x}_k^x \\ \mathbf{x}_k^v \\ \mathbf{x}_k^n \end{bmatrix} = \begin{bmatrix} \mathbf{x}_k \\ \mathbf{v}_k \\ \mathbf{n}_k \end{bmatrix}. \quad (15)$$

The corresponding covariance matrix \mathbf{P}_k^a is built from the individual covariances of \mathbf{x} , \mathbf{v} and \mathbf{n} :

Part 1: Retrieving state profiles with linear and nonlinear numerical schemes

G. B. Chirico et al.

Title Page

Abstract

Introduction

Conclusions

References

Tables

Figures

⏪

⏩

◀

▶

Back

Close

Full Screen / Esc

Printer-friendly Version

Interactive Discussion



$$\mathbf{P}_{x,k}^a = \begin{pmatrix} \mathbf{P}_{x_k} & 0 & 0 \\ 0 & \mathbf{R}_v & 0 \\ 0 & 0 & \mathbf{R}_n \end{pmatrix}. \quad (16)$$

Being L the dimension of the augmented vector, a *sigma* point set $\mathbf{S} = \{\mathbf{X}_i, \mu_i^{(j)}; i = 0 \dots 2L; j \in (m, c)\}$ is defined by $2L + 1$ sigma points \mathbf{X}_i , including the mean $\bar{\mathbf{x}}$, plus the respective mean (m) and covariance (c) weights $\mu_i^{(j)}$:

$$\begin{aligned} 5 \quad \mathbf{X}_0^a &= \bar{\mathbf{x}}^a \\ \mathbf{X}_i^a &= \bar{\mathbf{x}}^a + \left(\sqrt{\gamma \mathbf{P}_x^a}\right)_i \quad i = 1, \dots, L \\ \mathbf{X}_i^a &= \bar{\mathbf{x}}^a - \left(\sqrt{\gamma \mathbf{P}_x^a}\right)_i \quad i = L + 1, \dots, 2L \\ \mu_0^{(m)} &= \frac{\gamma - L}{\gamma} \\ \mu_0^{(c)} &= \frac{\gamma - L}{\gamma} + (1 - \rho^2 + \beta) \\ 10 \quad \mu_i^{(m)} &= \mu_i^{(c)} = \frac{1}{2\gamma} \quad i = 1, \dots, 2L. \end{aligned} \quad (17)$$

The parameter γ controls the spread of the sigma points around the mean, and is calculated as $\gamma = \rho^2(L + \kappa)$, with $\kappa \geq 0$ to ensure semi-positive definiteness of the covariance matrix and $0 \leq \rho \leq 1$. A good default choice is $\kappa = 0$ and ρ small enough to limit the spread of the sigma points. The parameter β is introduced as a second control on the magnitude of the covariance weights. Details about the proper choice of κ , ρ and β can be found in van der Merwe (2004). The symbol $\left(\sqrt{\gamma \mathbf{P}_x^a}\right)_i$ is the i -th column (or row) of the root square matrix $\gamma \mathbf{P}_x^a$, which can be regularly computed by Cholesky decomposition (e.g. Press et al., 1992).

Part 1: Retrieving state profiles with linear and nonlinear numerical schemes

G. B. Chirico et al.

Title Page

Abstract

Introduction

Conclusions

References

Tables

Figures

⏪

⏩

◀

▶

Back

Close

Full Screen / Esc

Printer-friendly Version

Interactive Discussion



At each time step, the $2L + 1$ σ points are calculated based on the current estimates of the expected state and covariance:

$$\mathbf{X}_{k-1}^a = \left[\hat{\mathbf{x}}_{k-1}^a \quad \hat{\mathbf{x}}_{k-1}^a + \sqrt{\gamma \mathbf{P}_{x,k-1}^a} \quad \hat{\mathbf{x}}_{k-1}^a - \sqrt{\gamma \mathbf{P}_{x,k-1}^a} \right]. \quad (18)$$

The sigma points are transformed through the dynamic system model:

$$\mathbf{X}_{k|k-1}^x = F(\mathbf{X}_{k-1}^x, \mathbf{X}_{k-1}^v, \mathbf{u}_{k-1}). \quad (19)$$

The transformed sigma points are weighted to gain an a priori estimate of the state mean and covariance as follows:

$$\hat{\mathbf{x}}_k^- = \sum_{i=0}^{2L} \mu_i^{(m)} \mathbf{X}_{i,k|k-1}^x \quad (20)$$

$$\mathbf{P}_{x_k}^- = \sum_{i=0}^{2L} \mu_i^{(c)} \left(\mathbf{X}_{i,k|k-1}^x - \hat{\mathbf{x}}_k^- \right) \left(\mathbf{X}_{i,k|k-1}^x - \hat{\mathbf{x}}_k^- \right)^T. \quad (21)$$

The sigma points are also transformed through the measurement model:

$$\mathbf{Y}_{k|k-1} = H(\mathbf{X}_{k-1}^x, \mathbf{X}_{k-1}^n) \quad (22)$$

which are then weighted to gain the a priori estimate of the measurement mean and covariance, as well as of the cross covariance between states and measurements:

$$\hat{\mathbf{y}}_k^- = \sum_{i=0}^{2L} \mu_i^{(m)} \mathbf{Y}_{i,k|k-1} \quad (23)$$

$$\mathbf{P}_{y_k}^- = \sum_{i=0}^{2L} \mu_i^{(c)} \left(\mathbf{Y}_{i,k|k-1} - \hat{\mathbf{y}}_k^- \right) \left(\mathbf{Y}_{i,k|k-1} - \hat{\mathbf{y}}_k^- \right)^T \quad (24)$$

$$\mathbf{P}_{x_k y_k}^- = \sum_{i=0}^{2L} \mu_i^{(c)} \left(\mathbf{X}_{i,k|k-1}^x - \hat{\mathbf{x}}_k^- \right) \left(\mathbf{Y}_{i,k|k-1} - \hat{\mathbf{y}}_k^- \right)^T. \quad (25)$$

Part 1: Retrieving state profiles with linear and nonlinear numerical schemes

G. B. Chirico et al.

Title Page

Abstract

Introduction

Conclusions

References

Tables

Figures

⏪

⏩

◀

▶

Back

Close

Full Screen / Esc

Printer-friendly Version

Interactive Discussion



The Kalman *gain* can be then computed with Eq. (4), while the a posteriori estimate of the state mean \hat{x}_{k-1}^a and covariance matrix \mathbf{P}_{x_k} can be computed respectively from Eqs. (3) and (5).

3 Soil water transport model

- 5 The soil water dynamics along the vertical direction is modelled using the Richards' equation (Jury et al., 1991) in the h -based form:

$$C(h) \frac{\partial h}{\partial t} = \frac{\partial [K(h) (\frac{\partial h}{\partial z} + 1)]}{\partial z} \quad (26)$$

10 where t is the time, z denotes the position along vertical axis (with upward orientation and zero reference value at the surface), h [L] is the matric pressure head [L], $K(h)$ [$L T^{-1}$] is the hydraulic conductivity function, and $C(h)$ [L^{-1}] is the differential water capacity function, obtained from the derivative $C(h) = d\theta(h)/dh$ of the water retention function $\theta(h)$ [$L^3 L^{-3}$].

The water retention and hydraulic conductivity functions are modelled according to the van Genuchten-Mualem model (van Genuchten, 1980):

$$15 \theta(h) = \theta_r + \theta_s - \theta_r [1 + |\alpha h|^n]^{-m} \quad (27)$$

$$K(\theta) = K_s \left(\frac{\theta - \theta_r}{\theta_s - \theta_r} \right)^\lambda \left\{ 1 - \left[1 - \left(\frac{\theta - \theta_r}{\theta_s - \theta_r} \right)^{1/m} \right]^m \right\}^2 \quad (28)$$

20 where θ_s is the saturated soil water content, θ_r is the residual soil water content, K_s is the saturated hydraulic conductivity, while $\alpha > 0$ [L^{-1}], $n > 1$ [-], m [-] and λ [-] are empirical parameters. Following a common assumption, parameter m [-] is defined by the relation $m = 1 - 1/n$ and λ [-] is fixed equal to 0.5.

A numerical scheme, integrating Eq. (26) and corresponding boundary conditions, is equivalent to a state-space description of the system model discretised in the time

Part 1: Retrieving state profiles with linear and nonlinear numerical schemes

G. B. Chirico et al.

Title Page	
Abstract	Introduction
Conclusions	References
Tables	Figures
◀	▶
◀	▶
Back	Close
Full Screen / Esc	
Printer-friendly Version	
Interactive Discussion	



domain, as in Eq. (1). Depending on the type of numerical scheme employed, the system model can be linear or nonlinear.

The measurement model could be reduced to a simple linear relation if matric pressure head is directly measured at given soil depths. If soil water content is measured, the observation equation is described by a nonlinear model corresponding to the soil water retention function, as Eq. (31). Other observation equations are required to assimilate other sources of measurements, such as those originated by near-surface remote sensing observations.

Below we illustrate three numerical schemes largely employed for integrating the Richards equation.

3.1 Explicit finite difference scheme (EX)

This is the numerical scheme employed by Walker et al. (2001), which is an explicit finite difference scheme, according to a forward Euler finite difference scheme. Writing Eq. (26) for node i at time-step $j + 1$ and vectorising, this numerical scheme provides an estimate of the matric potential h_i^{j+1} as function of all other quantities at the preceding time-step:

$$\left(h_i^{j+1} \right) = \left(\frac{\Delta t^j}{C_i^j} \frac{K_{i-1/2}^j}{\Delta z_j \Delta z_u}; 1 - \frac{\Delta t^j}{C_i^j} \frac{K_{i-1/2}^j + K_{i+1/2}^j}{\Delta z_j}; \frac{\Delta t^j}{C_i^j} \frac{K_{i+1/2}^j}{\Delta z_j \Delta z_l} \right) \begin{pmatrix} h_{i-1}^j \\ h_i^j \\ h_{i+1}^j \end{pmatrix} + \frac{\Delta t^j}{C_i^j} \frac{K_{i-1}^j - K_{i+1}^j}{2 \Delta z_j}. \quad (29)$$

The subscript i for the node number is increasing downward. The soil column is divided in compartments of finite thickness Δz_j . All nodes, including the top and bottom nodes, are in the centre of the soil compartments, with $\Delta z_u = z_{i-1} - z_i$ and $\Delta z_l = z_i - z_{i+1}$. This represents a small difference with respect to the work of Walker et al. (2001), who assumed nodes at the compartment extremes, positive upwards. $K_{i-1/2}^j$ and $K_{i+1/2}^j$ denotes respectively the upward and the downward spatial averages of the

Part 1: Retrieving state profiles with linear and nonlinear numerical schemes

G. B. Chirico et al.

Title Page

Abstract

Introduction

Conclusions

References

Tables

Figures

◀

▶

◀

▶

Back

Close

Full Screen / Esc

Printer-friendly Version

Interactive Discussion



hydraulic conductivity computed as arithmetic means. Δt^j indicates the time interval $\Delta t^j = t^{j+1} - t^j$.

The set of Eq. (29) written for each node, coupled with the boundary conditions, can be easily structured in matrix form to gather a state-space representation of the dynamic system as Eq. (1), with a linear model operator F described by a tri-diagonal matrix. The prediction step of the Kalman Filter can be implemented without any linearization, being the Jacobian matrices \mathbf{G} (Eq. 7) and \mathbf{L} (Eq. 8) coincident with F .

3.2 Crank-Nicolson finite difference scheme (CN)

The Crank-Nicolson implicit finite difference scheme (CN) has been widely implemented for solving the Richards equation (e.g. Haverkamp et al., 1977; Santini, 1980; Romano et al., 1998). Writing Eq. (26) for node i at time-step $j + 1$ and vectorising, yields:

$$\begin{aligned} & \left(-\frac{K_{i-1/2}^j}{2\Delta z_i \Delta z_u}; \frac{C_i^j}{\Delta t^j} + \frac{K_{i-1/2}^j}{\Delta z_u} + \frac{K_{i+1/2}^j}{\Delta z_l}; -\frac{K_{i+1/2}^j}{2\Delta z_i \Delta z_l} \right) \begin{pmatrix} h_{i-1}^{j+1} \\ h_{i+1}^{j+1} \\ h_{i+1}^{j+1} \end{pmatrix} \\ & = \left(\frac{K_{i-1/2}^j}{2\Delta z_i \Delta z_u}; \frac{C_i^j}{\Delta t^j} - \frac{K_{i-1/2}^j}{\Delta z_u} + \frac{K_{i+1/2}^j}{\Delta z_l}; \frac{K_{i+1/2}^j}{2\Delta z_i \Delta z_l} \right) \begin{pmatrix} h_{i-1}^j \\ h_i^j \\ h_{i+1}^j \end{pmatrix} + \frac{K_{i-1}^j - K_{i+1}^j}{2\Delta z_i}. \quad (30) \end{aligned}$$

As in the previous algorithm, an explicit linearization of K and C is implemented, by taking their values at the previous time-step j . A linear state-space representation of the dynamic system can be easily derived by combining the set of Eq. (30) written for each node and accounting for the boundary conditions:

$$\mathbf{A}_{(K_k, C_k, z, t)} \mathbf{x}_{k+1} = \mathbf{B}_{(K_k, C_k, z, t)} \mathbf{x}_k + \mathbf{g}_{(K_k, \beta_{top_k}, \beta_{bot_k}, z, t)}. \quad (31)$$

Part 1: Retrieving state profiles with linear and nonlinear numerical schemes

G. B. Chirico et al.

Title Page

Abstract

Introduction

Conclusions

References

Tables

Figures

◀

▶

◀

▶

Back

Close

Full Screen / Esc

Printer-friendly Version

Interactive Discussion



A and **B** are tri-diagonal matrices and **g** is a vector. The symbols in parenthesis remind the variables occurring in the elements of **A**, **B** and **g**. The symbols β^{top} and β^{bot} indicate the top and bottom boundary conditions. The state variable **x** is the matrix pressure head. As with the forward Euler scheme, the prediction phase of the Kalman Filter can be implemented without any linearization. An a priori estimate \hat{x}_k^- can be obtained by solving Eq. (31), which does not require any iteration, but it involves the inversion of matrix **A**. The model operator *F* is linear, fully defined by the matrix $\mathbf{F} = \mathbf{A}^{-1} \mathbf{B}$.

3.3 Nonlinear implicit finite difference scheme (NL)

A nonlinear implicit finite difference (NL) scheme, according to a backward Euler scheme, has been introduced by Celia et al. (1990) and further implemented by the SWAP model (van Dam, 2001), to account for the high nonlinearity of the differential water capacity *C*. The numerical scheme includes the *C* values at the current time-step *j* + 1:

$$\begin{aligned} & \left(\begin{array}{c} -\frac{K_{i-1/2}^j}{\Delta Z_i \Delta Z_u}; \frac{C_i^{j+1,p-1}}{\Delta t^j} + \frac{K_{i-1/2}^j}{\Delta Z_u} + \frac{K_{i+1/2}^j}{\Delta Z_l}; -\frac{K_{i+1/2}^j}{\Delta Z_i \Delta Z_l} \end{array} \right) \begin{pmatrix} h_{i-1}^{j+1,p} \\ h_i^{j+1,p} \\ h_{i+1}^{j+1,p} \end{pmatrix} \\ & = \frac{C_i^{j+1,p-1}}{\Delta t^j} h_i^{j+1,p-1} + \frac{K_{i-1}^j - K_{i+1}^j}{2 \Delta Z_i} + \theta_i^j - \theta_{i-1}^{j+1,p-1}. \end{aligned} \quad (32)$$

This type of numerical scheme requires an iterative solution. The index *p* denotes the iteration level. In this case, the system of Eq. (32), written for each node and combined with the boundary conditions, corresponds to a state-space representation of the dynamic system with a nonlinear operator *F*, which implies the implementation of non-standard Kalman Filters, such as the EKF and the UKF, for the a priori \hat{x}_k^- and $\mathbf{P}_{x_k}^-$ predictions.

Part 1: Retrieving state profiles with linear and nonlinear numerical schemes

G. B. Chirico et al.

Title Page

Abstract

Introduction

Conclusions

References

Tables

Figures

⏪

⏩

◀

▶

Back

Close

Full Screen / Esc

Printer-friendly Version

Interactive Discussion



4 Synthetic study

A synthetic study is performed to evaluate the relative merits of different Kalman Filters assimilation algorithms for retrieving pressure head profiles from near surface pressure head or water content measurements.

As pointed out above, the type of Kalman Filters applicable is limited by the numerical scheme employed. The Standard Kalman Filter (SKF) can be implemented with explicit (EX) and Crank-Nicolson (CN) finite difference schemes, as far as the measurement model is linear. In the study case, a linear measurement model occurs if the measured variable is the matric pressure head h . If soil water content is the measured variable, a non-standard Kalman Filter is required to overcome the nonlinearity the measurement model H defined by the soil water retention function. Non-standard Kalman Filters are also required if a nonlinear implicit finite difference scheme (NL) is employed.

Walker et al. (2001) showed the efficiency of a standard Kalman Filter (SKF) in assimilating near surface pressure head measurements with an explicit finite difference scheme (EX) as compared with direct insertion of the observation values. The Authors implemented a specific SKF algorithm (hereafter SKF_v), without transforming the process noise v through the dynamic system model F , as illustrated in Eqs. (13) and (14).

Following Walker et al. (2001), we first compare the efficiency of SKF_v implemented with a Crank-Nicolson finite difference scheme (SKF_v -CN), to the SKF_v implemented with an explicit finite difference scheme (SKF_v -EX). Then we compare the Unscented Kalman Filter (UKF) with an implicit nonlinear finite difference scheme (UKF-NL), to a SKF-CN assimilation algorithm.

Finally, we examine the case when soil water content is the measured variable, by comparing the UKF-NL assimilation scheme with the EKF-CN assimilation scheme. Table 1 summarizes the assimilation schemes adopted.

Part 1: Retrieving state profiles with linear and nonlinear numerical schemes

G. B. Chirico et al.

Title Page

Abstract

Introduction

Conclusions

References

Tables

Figures



Back

Close

Full Screen / Esc

Printer-friendly Version

Interactive Discussion



4.1 Numerical experiment

The soil water transfer model illustrated above (Eqs. 26–28) has been used to generate a set of soil water content and matric head profiles, representative of the true dynamic process to be retrieved. The numerical experiment is arranged equally to that implemented by Walker et al. (2001), to facilitate the comparison with this previous study.

The essential information of the implemented numerical experiment is summarized in Table 2. Soil column depth is 100 cm, discretised in 27 nodes and the true initial matric pressure head profile is uniform and equal to -50 cm. The boundary conditions are: constant evaporative flux of $5.78 \times 10^{-6} \text{ cm s}^{-1}$ at the top surface and no flux at the bottom. Matric pressure head h profiles are then retrieved by assimilating hourly h data generated within the first 0.5, 1.5, 4.5 and 10 cm. These depths are slightly different from those adopted by Walker et al. (2001), because of the small differences in the soil column discretisation, as illustrated in Sect. 3.1. All assimilation schemes are initialized with the same poor guess of the initial matric pressure head profile, assumed uniformly equal to -300 cm, thus 250 cm less than the true initial uniform profile.

Two main differences occur in the implemented assimilation schemes, with respect to previous work by Walker et al. (2001).

First, the default initial state variance is fixed to 10^3 cm^2 , rather than 10^6 used by Walker et al. (2001), since using an extremely high initial state variance causes practical difficulties in the implementation of the UKF, as discussed later.

Second, the amount of system noise variance is implemented in a different way. Walker et al. (2001) assumed a five percent of the change of the state for the diagonal elements matrix, and zero for those off-diagonal. Entekhabi et al. (1994), considered an “initially diagonal” matrix accounting for the five percent of the precedent state. We employed the second approach, as it is more realistic and it also ensures that noise variances are not affected by the number of time steps between observations

Part 1: Retrieving state profiles with linear and nonlinear numerical schemes

G. B. Chirico et al.

Title Page

Abstract

Introduction

Conclusions

References

Tables

Figures



Back

Close

Full Screen / Esc

Printer-friendly Version

Interactive Discussion

Thus, also for comparison purposes, we adopted a diagonal system noise variance, accounting for the five percent of the previous hourly a posteriori state.

4.2 Comparison of SKF_v -EX and SKF_v -CN assimilation algorithms

In Fig. 1, the true profiles are compared with the profiles retrieved with the SKF_v -EX and SKF_v -CN assimilation algorithms, respectively, as well as with the “guess” profile. The “guess” profile is the one obtained without assimilating any near-surface observations, i.e. the system is simply propagated from the initial conditions using the known boundary conditions.

The two sets of profiles retrieved by using the SKF_v algorithm respectively coupled with the explicit and the Crank-Nicolson numerical schemes, are almost identical. However, the explicit scheme, in order to guarantee numerical accuracy and stability, requires time steps of the order of few seconds, turning unreliable in operational applications. The CN scheme, instead, allows for time steps of the order of hundreds of seconds, saving considerable amount of computational time. Another favourable aspect with the CN scheme is that, being particularly stable, it is able to retrieve the true profile, even for a decreased precision of the model equation.

In Walker et al. (2001), the retrieved profiles coincided with the true ones within 12 h after the beginning of the assimilation process, thus in a time interval smaller than in the present numerical experiment. This difference is basically due to the fact that the initial state covariance matrix herein employed is by two orders smaller than the one in Walker et al. (2001). As shown by Walker (1999) in a sensitivity analysis for the same experimental setup, the convergence time tends to increase as one takes higher initial state covariance values.

Walker (1999) also found that the performance of the retrieved algorithm is not particularly sensible to the system noise variance. However, this result should be interpreted keeping in mind that Walker (1999) assumed the system noise variance equal to five percent of the state change. Instead, in the present study, the system noise variance

Part 1: Retrieving state profiles with linear and nonlinear numerical schemes

G. B. Chirico et al.

Title Page

Abstract

Introduction

Conclusions

References

Tables

Figures



Back

Close

Full Screen / Esc

Printer-friendly Version

Interactive Discussion

has a more important role, as it is assumed equal to five percent of the previous state, accordingly with Entekhabi (1994).

4.3 Comparison of SKF-CN and UKF-NL assimilation algorithms

Provided that the SKF_v-CN assimilation algorithm is much more efficient than the SKF_v-EX algorithm from a computational perspective, the SKF-CN assimilation algorithm has been then compared with the UKF applied to the implicit nonlinear numerical scheme of the Richards equation (UKF-NL).

Alternatively to the UKF, the EKF could be also employed in conjunction with a nonlinear numerical scheme of the Richards equation. However, the EKF, based on an explicit linearization of nonlinear equations, is less efficient in state retrieving as compared with UKF. The work of Entekhabi et al. (1994), who implemented the EKF with a finite elements algorithm, testifies that the EKF demands more time in retrieving the true profiles than ordinarily observed in the present work with different KF algorithms for analogous case studies. Further discussions about the limitations and the flaws of the EKF can be found in other studies (e.g. Julier et al., 1995; van der Merwe, 2004).

In the UKF-NL algorithm, the nonlinear implicit differential scheme of the Richards equation is solved for each sigma point to predict its state evolution, while the overall state mean and covariance are calculated just before the observation is available. Given the hourly periodicity of the observations in this synthetic experiment, the nonlinear implicit differential scheme is resolved with an hourly time-step, thanks to its high numerical stability and accuracy. The LKF-CN algorithm is instead implemented with a time step of 200 s.

The UKF strategy of augmenting the state random variable with the noise random variables entails that the uncertainty of the noise covariance is taken into account similarly to that of state vector during the sigma-point propagation. In other words, the dynamic operator acts simultaneously on both the system state covariance and the noise covariance. The same effect is achieved with the SKF-CN algorithm, where the dynamic equation assumes the following equation:

Part 1: Retrieving state profiles with linear and nonlinear numerical schemes

G. B. Chirico et al.

Title Page

Abstract

Introduction

Conclusions

References

Tables

Figures



Back

Close

Full Screen / Esc

Printer-friendly Version

Interactive Discussion



$$\mathbf{A}_{(K^k, C^k, z, t)} \mathbf{x}^{k+1} = \mathbf{B}_{(K^k, C^k, z, t)} \left(\mathbf{x}^k + \mathbf{v}^k \right) + \mathbf{f}_{(K^k, K^k, Q_{top}, Q_{bot}, z, t)} \quad (33)$$

The a priori estimate of the covariance matrix is thus calculated as follows:

$$\hat{\mathbf{P}}_{x_{k+1}}^- = \left(\mathbf{A}_k^{-1} \mathbf{B}_k \right) \mathbf{P}_{x_k} \left(\mathbf{A}_k^{-1} \mathbf{B}_k \right)^T + \left(\mathbf{A}_k^{-1} \mathbf{B}_k \right) \mathbf{Q}_k \left(\mathbf{A}_k^{-1} \mathbf{B}_k \right)^T \quad (34)$$

where \mathbf{Q}_k is set as the five percent of the previous posterior mean state.

As anticipated above, this approach differs from the one implemented by Walker et al. (2001), corresponding to the SKF_v-CN algorithm, which can be formally described as:

$$\mathbf{A}_{(K^k, C^k, z, t)} \mathbf{x}^{k+1} = \mathbf{B}_{(K^k, C^k, z, t)} \left(\mathbf{x}^k \right) + \mathbf{f}_{(K^k, K^k, Q_{top}, Q_{bot}, z, t)} + \mathbf{v}^k \quad (35)$$

giving place to:

$$\hat{\mathbf{P}}_{x_{k+1}}^- = \left(\mathbf{A}_k^{-1} \mathbf{B}_k \right) \mathbf{P}_{x_k} \left(\mathbf{A}_k^{-1} \mathbf{B}_k \right)^T + \mathbf{Q}_k. \quad (36)$$

These differences in the way of assuming the error are scarcely transcendent in the domain of a few hours of simulation, but become important when the frequency of the observations significantly decreases to one every several days, as could be in practical circumstances.

Figure 2 shows the retrieved profiles by assimilating near surface hourly observations using the SKF-CN and UKF-NL algorithms, assuming an evolving structure of the system noise covariance as in Eq. (34), with two alternative initial system state variances, 10^3 and 10^4 cm^2 .

With SKF-CN, complete retrieving of the true profile took around 20 h in the case of pressure head assimilation. The differences between retrieved profiles, using either 10^3 or 10^4 cm^2 as diagonal elements of the initial state variance, are small.

Part 1: Retrieving state profiles with linear and nonlinear numerical schemes

G. B. Chirico et al.

Title Page

Abstract

Introduction

Conclusions

References

Tables

Figures

⏪

⏩

◀

▶

Back

Close

Full Screen / Esc

Printer-friendly Version

Interactive Discussion



Contrary to the SKF-CN, the UKF-NL algorithm exhibits a marked sensitivity to the initial state variance. Complete retrieval of the true profiles is achieved in a shorter time interval with larger initial state variance: 12 h with 10^4 cm^2 as initial state variance, while 18 h with 10^3 cm^2 as initial state variance.

This ostensibly better behaviour of the UKF when using higher initial state variance is mainly favoured by the bias in the estimation of the prior mean state, which can actually determine some difficulties in the implementation of the UKF algorithm. Indeed, this approach lies on a deterministic sampling of sigma points around the mean, whose distribution logically depends on the magnitude of the variance. Taking a very high initial variance, without any correlation structure, could lead to sample profiles which are physically improbable, and consequently the stability of the assimilation process could degenerate.

This issue can be overcome by shrinking the sigma point distribution around the mean state with the scaling parameter ρ , which controls the weights attributed to the sigma point distribution (Eq. 20). Values of ρ close to zero translate into a considerably increase (in absolute terms) of the sigma points weights, which favours the cited bias.

Figure 3 shows a comparison between the UKF prior mean state estimated using $\rho = 0.05$, $\rho = 0.3$ and $\rho = 0.8$ in Eq. (20), and the evolution of the central state after the first hour update, assuming both initial state variances equal to 10^3 and 10^4 cm^2 on the diagonal elements. The prior mean state estimation using the smaller initial state variance value is practically insensitive to the value of ρ , while this prior mean is highly affected by ρ when using the higher initial state variance. Taking $\rho = 0.8$, with a uniform initial profile -300 cm and state variance of 10^4 cm^2 , leads to a set of sampled profiles (sigma points) exhibiting positive pressure heads for perturbed nodes. Instead, using 0.05 magnifies the weights and thus enhances the asymmetry in the sigma points distribution.

In practical applications, particularly those where the frequency of the observations is small, the evolution of the magnitudes of the state variance is unpredictable. Thus, the coefficients selected for designing the sigma point sampling strategy could turn out

Part 1: Retrieving state profiles with linear and nonlinear numerical schemes

G. B. Chirico et al.

Title Page

Abstract

Introduction

Conclusions

References

Tables

Figures

⏪

⏩

◀

▶

Back

Close

Full Screen / Esc

Printer-friendly Version

Interactive Discussion



inadequate during the assimilation process. To overcome this issue, some other UKF applications adapt the value of the coefficients to guaranty the physical coherence of the sample states.

These types of issues are not encountered with the SKF-CN algorithm, as mean and variance run independently.

Another limitation of the UKF with respect to the SKF is the computational effort. Being L the dimension of the augmented state vector (in this case equal two times the number N of nodes in which the soil column is discretised, plus the number of observation nodes), the differential equations of the dynamic model need to be executed $2L + 1$ times during each time step for obtaining a priori estimates of the mean and variance. For long time applications this can mean a relevant computational effort. An option for minimizing this problem is to optimize the discretisation of the soil column.

On the other hand, one aspect favouring the application of the UKF is the possibility to implement straightforwardly nonlinear state variable transformations. When states are very far from observations, the filtering process imposes severe gradients in the profiles, propitiating the estimation of temporary meaningless profiles. This could be partially avoided by making a transformation of the state (e.g. logarithmic), which implies at the same time a nonlinear transformation of the dynamic equation. This transformation, scarcely affecting the UKF results (not shown), should be treated by linearization of an already linearized equation in the case of an Extended Kalman Filter, therefore with a drastic reduction of the efficiency of the assimilation algorithm.

Figure 4 shows the retrieved profiles by assimilating soil water potential observations once every two days. In both cases the initial state covariance employed has been set to 10^3 cm^2 . To guarantee a performance of the UKF comparable with that of SKF, the parameter ρ has been specifically tuned. Results show that the SKF is able to retrieve the true profile already at the fourth day, i.e. at the second assimilation, practically for any observation depths. Satisfactory results with the SKF have been also obtained (not shown here) by assimilating observations once every tree days and four days, except the case when the observations are limited to the top node. SKF failed only for larger

Part 1: Retrieving state profiles with linear and nonlinear numerical schemes

G. B. Chirico et al.

Title Page

Abstract

Introduction

Conclusions

References

Tables

Figures



Back

Close

Full Screen / Esc

Printer-friendly Version

Interactive Discussion



observation time-intervals, as the extremely negative pressured heads of the predicted states at the top nodes altered the singularity of matrix operators. To achieve results analogue to those obtained with SKF, specific tunings of the assimilation scheme are required with the UKF.

5 4.4 Assimilation of soil water content observations

The analysis has been also extended to examine the case of assimilating soil water content observations, instead of matric pressure heads. In this case the CN numerical scheme has been coupled with an EKF, entailing the computation of the Jacobians matrices of the observation equation, in order to deal with the nonlinearity of the soil water retention function. Figure 5 represents the analogue comparison with those shown in Fig. 2, but assimilating soil water content observations instead of soil water potential values.

With EKF-CN, complete retrieving of the true profile occurs only around the fourth day, thus after a time much longer than that required by assimilating pressure head observations with SKF-CN.

The effect of different observation depths is much more evident when taking soil water content instead of soil water potential values as observations. Moreover, with the UKF-NL algorithm, the effect of the initial state variance on the retrieving performance is even more accentuated when assimilating soil water content values than matric pressure heads. In this case, complete retrieving required 4 days taking 10^4 cm^2 as initial state variance, while 8 days assuming 10^3 cm^2 as initial state variance.

It is important to point out that the results obtained by assimilating soil water content values, are subjected to the assumption that the parameters defining the soil water retention at the observation points coincide with those employed for simulating the soil water dynamics along the entire soil column considered as homogeneous. However, in practical circumstances, the retrieving process should account for the system heterogeneity and model simplifications of the real-world soil hydrological processes. The “optimal” parameters defining the soil water retention at the observation points are in

Part 1: Retrieving state profiles with linear and nonlinear numerical schemes

G. B. Chirico et al.

Title Page

Abstract

Introduction

Conclusions

References

Tables

Figures



Back

Close

Full Screen / Esc

Printer-friendly Version

Interactive Discussion



principle different from the “optimal” parameters defining the soil water dynamics along the soil column. These “optimal” soil hydraulic parameters are to be considered as effective values at the scales of the observation or of the modelled system, respectively (Vereecken et al., 2007).

5 4.5 Dynamic evolution of the state covariance

Figure 6 shows how the variances explained by the first two principal components (PC) of the state covariance evolve, considering the simulations during the first 24 hours for pressure head assimilations, and 72 hours for soil water content assimilations, with two different initial state covariance matrices, 10^3 and 10^4 cm².

10 Figure a and b shows the evolution of the explained covariance with the application of SKF_v-EX and SKF_v-CN schemes, respectively. Both PCs initially increase up to around the tenth observation. At this stage a low cross-covariance establishes between top nodes, already retrieved to the true small (in terms of absolute value) pressure heads, while a high cross-covariance occurs between the deepest nodes, still far from the true profile. Thus, the explained variance of the first PC (PC 1) tends to rapidly increase while that of the second PC (PC 2) decreases. This trend is also favoured by a system noise covariance punishing the higher state values. Once the retrieved profiles reach the true values for the entire depths, the explained variance of PC 1 reaches the maximum value. After this point, additional contributions from the system noise error, according to the SKF_v scheme, entails a reduction of the total variance explained by the first two components to values less than 50%. With smaller initial state covariance, the maximum explained variance of PC 1 tends to markedly reduce and the effect of observation depth also starts to be clearer.

25 As shown by Fig. 6c and d, the influence of the observation depths practically disappears when employing the UKF-NL and the SKF-CN schemes. The different patterns observed for UKF-NL and LKF-CN are not only due to the anomalous behaviour observed for the updated UKF prior mean profiles with the higher initial state variance, but also to the difference between the corresponding computational time-steps, which

Part 1: Retrieving state profiles with linear and nonlinear numerical schemes

G. B. Chirico et al.

Title Page

Abstract

Introduction

Conclusions

References

Tables

Figures



Back

Close

Full Screen / Esc

Printer-friendly Version

Interactive Discussion



determines a different interaction of the system noise covariance with the state covariance. Figure 6c shows that, using the SKF-CN scheme for assimilating pressure head, the percent of explained variance is highly influenced by the initial state variance, although the response of the mean state is poorly sensible, as shown in Fig. 2.

This analysis also demonstrates the implications of assuming a structure of the system noise covariance according to the SKF-CN scheme, as presented in Eq. (33), and not to the SKF_v-CN scheme, as presented in Eq. (33). During pressure head assimilations, once a total predominance of the first PC is reached, the additional supply from the system noise error makes the path described by the first two PCs to turn back along a similar trajectory, which provides a more “natural” updating, differently from the SKF_v-CN case, which instead leads to a reduction of the explained variance, following a different trajectory. This way of assuming the noise variance allowed for a very good behaviour of the SKF-CN algorithm even with much less frequent observations, without recurring to alternative strategies as those evaluated by Walker et al. (2001).

In case of soil water content observations, introducing a nonlinear observation equation propitiates a larger influence of the observation depth on the state covariance, for both the EKF-CN and the UKF-NL algorithms. The influence assimilated variable of the initial state variance on the evolution of the PC variances becomes less noticeable, particularly for the EKF-CN algorithm.

5 Conclusions

The analyses carried out in this study demonstrate that when designing a Kalman Filter algorithm for assimilating near surface data in the Richards equation, the Kalman Filter itself should be chosen considering the numerical scheme employed for solving the Richards equation, the form (“*h*-based” or “*θ*-based”) of this equation, and the type of assimilated variable.

A general guideline is to choose the form of the Richards equation according to the assimilated variable, so that the type of variable describing the observations is equal to

Part 1: Retrieving state profiles with linear and nonlinear numerical schemes

G. B. Chirico et al.

Title Page

Abstract

Introduction

Conclusions

References

Tables

Figures



Back

Close

Full Screen / Esc

Printer-friendly Version

Interactive Discussion



Part 1: Retrieving state profiles with linear and nonlinear numerical schemes

G. B. Chirico et al.

Title Page

Abstract

Introduction

Conclusions

References

Tables

Figures

⏪

⏩

◀

▶

Back

Close

Full Screen / Esc

Printer-friendly Version

Interactive Discussion



- Milly, P. C. and Dunne, K. A.: Sensitivity of the global water cycle to the water-holding capacity of land, *J. Climate*, 7, 506–526, 1994.
- Press, W. H., Teukolsky, S. A., Vetterling, W. T., and Flannery, B. P.: *Numerical Recipes in C: The Art of Scientific Computing*, 2nd Edn., Cambridge University Press, 1992.
- 5 Rodriguez-Iturbe, I. and Porporato, A.: *Ecohydrology of Water-Controlled Ecosystems: Soil Moisture and Plant Dynamics*, Cambridge University Press, 2005.
- Romano, N., Brunone, B., and Santini, A.: Numerical analysis of one-dimensional unsaturated flow in layered soils, *Adv. Water Resour.*, 21, 315–324, 1998.
- Santini, A.: Model for simulating soil water dynamics considering root extraction. Proceedings of CCE Seminaires sur l'Irrigation Localisee – Agrimed Sorrento, Italy, 1980.
- 10 van Dam, J. C.: Field-scale water flow and solute transport, SWAP model concepts, parameter estimation and case studies, Doctoral Thesis Wageningen University, 2000.
- van der Merwe, R.: *Sigma-Point Kalman Filters for Probabilistic Inference in Dynamic State-Space Models*, PhD dissertation, University of Washington, USA, 2004.
- 15 van Genuchten, M. Th.: A closed-form equation for predicting the hydraulic conductivity of unsaturated soils, *Soil Sci. Soc. Am. J.*, 44, 892–898, 1980.
- Vereecken, H., Kasteel, R., Vanderborght, J., and Harter, T.: Upscaling hydraulic properties and soil water flow processes in heterogeneous soils, *Vadose Zone J.*, 6, 1–28, doi:10.2136/vzj2006.0055, 2007.
- 20 Vereecken, H., Huisman, J. A., Bogena, H., Vanderborght, J., Vrugt, J. A., and Hopmans, J. W.: On the value of soil moisture measurements in vadose zone hydrology: A review, *Water Resour. Res.*, 44, W00D06, doi:10.1029/2008WR006829, 2008.
- Vogel, T., Huang, K., Zhang, R., van Genuchten, M. T.: The HYDRUS code for simulating one-dimensional water flow, solute transport and heat movement in variably-saturated media, Research Report No. 140, US Salinity Laboratory, Agricultural Research Service, USDA, Riverside, CA, 1996.
- 25 Walker, J. P.: Estimating soil moisture profile dynamics from near-surface soil moisture measurements and standard meteorological data, Ph.D. thesis, The University of Newcastle, Callaghan, New South Wales, Australia, 766 pp., 1999.
- 30 Walker, J. P., Willgoose, G. R., and Kalma, J. D.: One-dimensional soil moisture profile retrieval by assimilation of near-surface observations: a comparison of retrieval algorithms, *Adv. Water Resour.*, 24, 631–650, 2001.

Part 1: Retrieving state profiles with linear and nonlinear numerical schemes

G. B. Chirico et al.

Table 1. Summary of assimilation algorithms adopted in combination with different numerical schemes and different types of observed variables.

Observed variable	Finite difference scheme		
	EX	CN	NL
h	SKF _{ν} ^b	SKF ^a	UKF ^d
θ	–	EKF ^c	UKF ^d

^a SKF, standard Kalman Filter; ^b SKF _{ν} , SKF without transforming the process noise ν through the dynamic system Eqs. (13) and (14); ^c EKF, Extended Kalman Filter; ^d UKF unscented Kalman Filter.

Title Page

Abstract

Introduction

Conclusions

References

Tables

Figures

⏪

⏩

◀

▶

Back

Close

Full Screen / Esc

Printer-friendly Version

Interactive Discussion



Part 1: Retrieving state profiles with linear and nonlinear numerical schemes

G. B. Chirico et al.

Table 2. Parameters and conditions employed in the synthetic generation of pressure head profiles and for the initialization of the assimilation algorithms.

Soil depth	100 cm
Number of nodes	27
Soil hydraulic parameters	$\theta_s = 0.54 \text{ cm}^3 \text{ cm}^{-3}$ $\theta_r = 0.2 \text{ cm}^3 \text{ cm}^{-3}$ $\alpha = 0.008 \text{ cm}^{-1}$ $n = 1.8 (-)$ $K_s = 2.9 \times 10^{-4} \text{ cm}^{-1}$
Top flux	$5.79 \times 10^{-6} \text{ cm s}^{-1}$
Bottom flux	0 cm s^{-1}
Initial uniform h profile	-50 cm
Poor guess of initial uniform h profile	-300 cm
Initial state covariance matrix	$\mathbf{P}_{x,i,j} = \begin{cases} 10^3 \text{ cm}^2 & \text{if } i = j; i, j = 1 \dots n_nodes \\ 0 \text{ cm}^2 & \text{if } i \neq j \end{cases}$
Measurement noise variance matrix	$\mathbf{R}_{i,j} = \begin{cases} 0.02 y_i \text{ cm}^2 & \text{if } i = j; i, j = 1 \dots n_obs \\ 0 \text{ cm}^2 & \text{if } i \neq j \end{cases}$

Title Page

Abstract

Introduction

Conclusions

References

Tables

Figures

⏪

⏩

◀

▶

Back

Close

Full Screen / Esc

Printer-friendly Version

Interactive Discussion



Part 1: Retrieving state profiles with linear and nonlinear numerical schemes

G. B. Chirico et al.

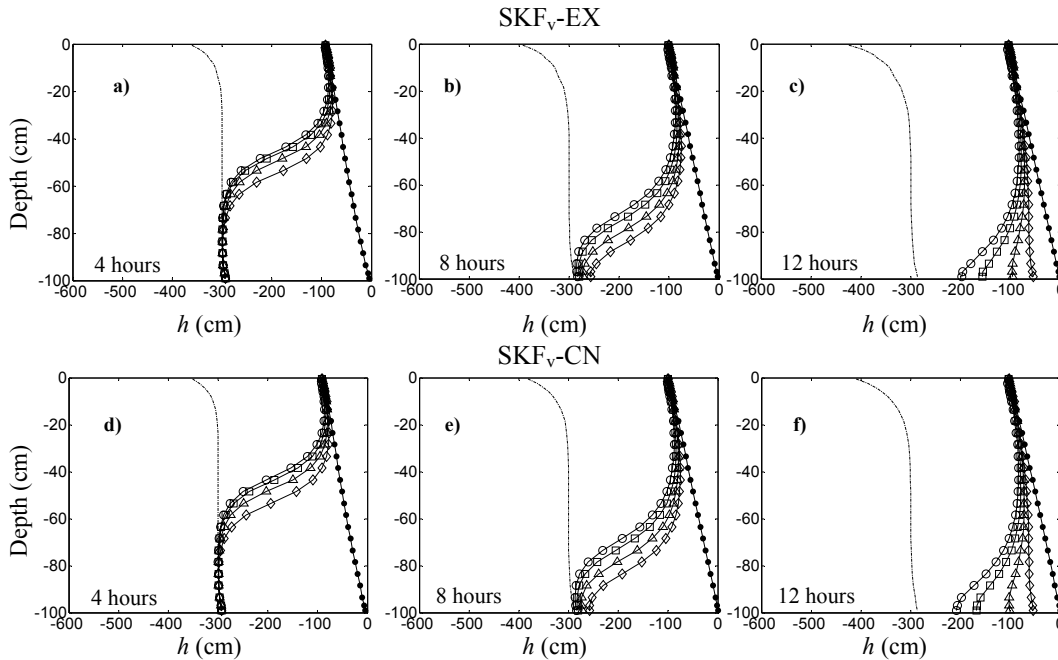


Fig. 1. Retrieved profiles by assimilating hourly observations of pressure heads involving nodes within the top 0.5 cm (open circle), 1.5 cm (square), 4.5 cm (triangle) and 10.5 cm (diamond) compared with the “true” profile (closed circle) and “guess” profile (dashed line). The top panels show the results obtained with the SKF_v-EX, while the bottom panels show those obtained with SKF_v-CN after (a)–(d) 4 h, (b)–(e) 8 h and (c)–(f) 12 h, respectively.

Title Page

Abstract Introduction

Conclusions References

Tables Figures

◀ ▶

◀ ▶

Back Close

Full Screen / Esc

Printer-friendly Version

Interactive Discussion



Part 1: Retrieving state profiles with linear and nonlinear numerical schemes

G. B. Chirico et al.

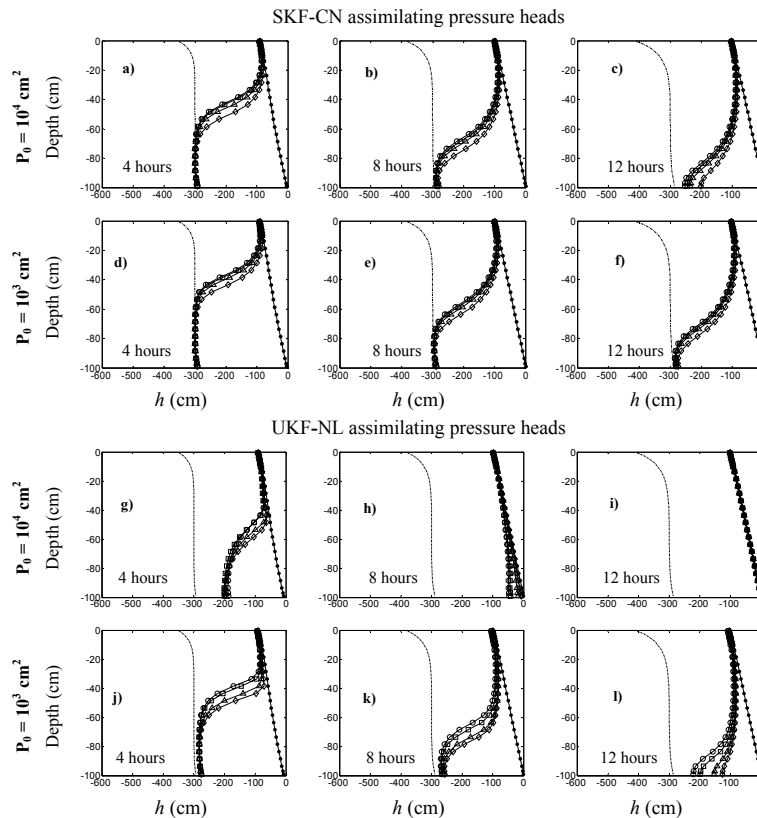


Fig. 2. Retrieved profiles by assimilating hourly observations of pressure heads involving nodes within the top 0.5 cm (open circle), 1.5 cm (square), 4.5 cm (triangle) and 10.5 cm (diamond) compared with the “true” profile (closed circle) and “guess” profile (dashed line) using **(a)–(f)** the SKF-CN algorithm and **(g)–(l)** using UKF-NL algorithm, with initial state covariance matrices $P_0 = 10^3 \text{ cm}^2$ and 10^4 cm^2 .

[Title Page](#)
[Abstract](#)
[Introduction](#)
[Conclusions](#)
[References](#)
[Tables](#)
[Figures](#)
[◀](#)
[▶](#)
[◀](#)
[▶](#)
[Back](#)
[Close](#)
[Full Screen / Esc](#)
[Printer-friendly Version](#)
[Interactive Discussion](#)

Part 1: Retrieving state profiles with linear and nonlinear numerical schemes

G. B. Chirico et al.

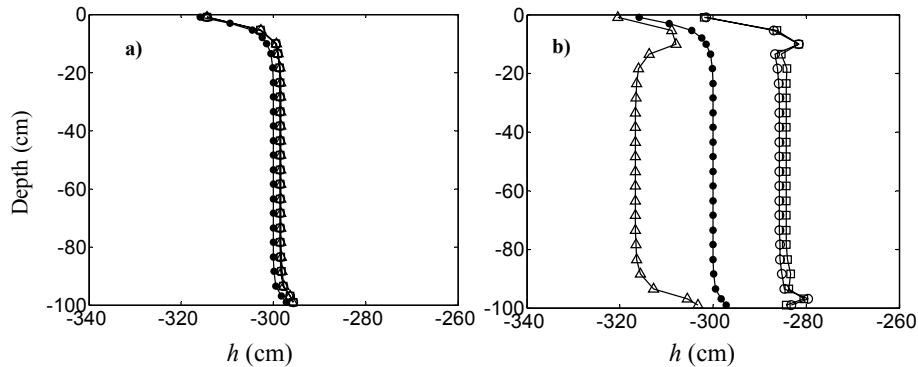


Fig. 3. Comparison between the UKF-NL prior mean state estimated using $\rho = 0.05$ (open circle), $\rho = 0.3$ (open square) and $\rho = 0.8$ (triangle) in Eq. (20), and the evolution of the central state (closed circle) after the first hourly update, considering initial state covariance values **(a)** $P_0 = 10^3 \text{ cm}^2$ and **(b)** $P_0 = 10^4 \text{ cm}^2$.

[Title Page](#)[Abstract](#)[Introduction](#)[Conclusions](#)[References](#)[Tables](#)[Figures](#)[◀](#)[▶](#)[◀](#)[▶](#)[Back](#)[Close](#)[Full Screen / Esc](#)[Printer-friendly Version](#)[Interactive Discussion](#)

Part 1: Retrieving state profiles with linear and nonlinear numerical schemes

G. B. Chirico et al.

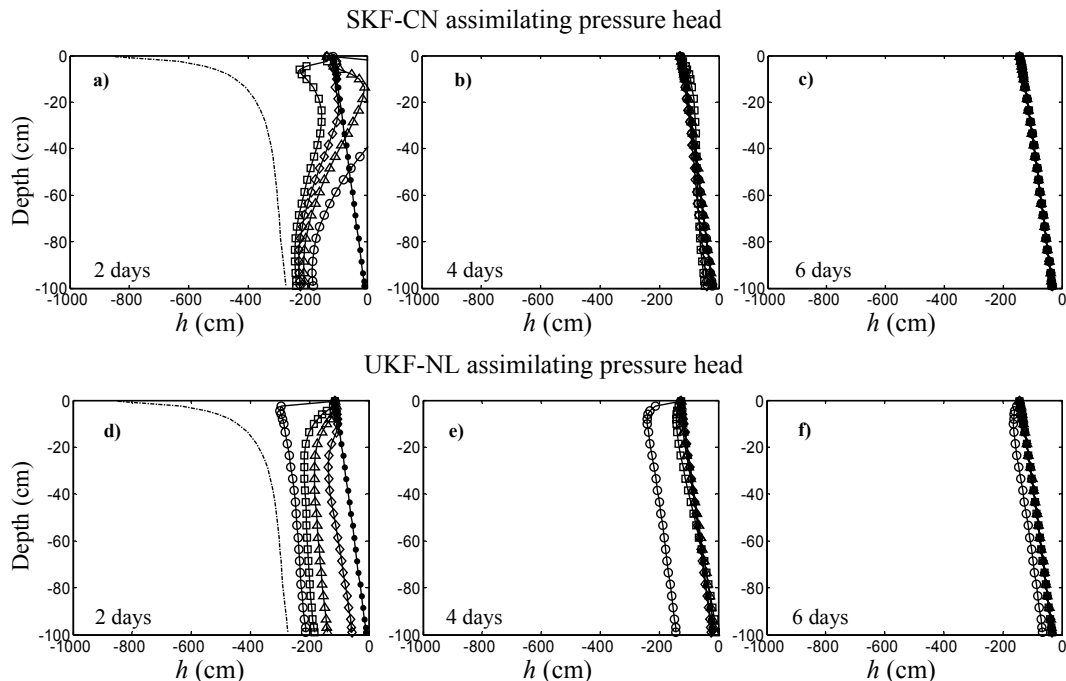


Fig. 4. Retrieved profiles after (a)–(d) 2 days; (b)–(e) 4 days, and (c)–(f) 6 days using SKF-CN and UKF-NL, respectively, by assimilating pressure head observations every two days involving the nodes within the top 0.5 cm (open circle), 1.5 cm (square), 4.5 cm (triangle) and 10.5 cm (diamond), as compared with the “true” profile (closed circle) and “guess” profile (dashed line).

Title Page

Abstract Introduction

Conclusions References

Tables Figures

◀ ▶

◀ ▶

Back Close

Full Screen / Esc

Printer-friendly Version

Interactive Discussion



Part 1: Retrieving state profiles with linear and nonlinear numerical schemes

G. B. Chirico et al.

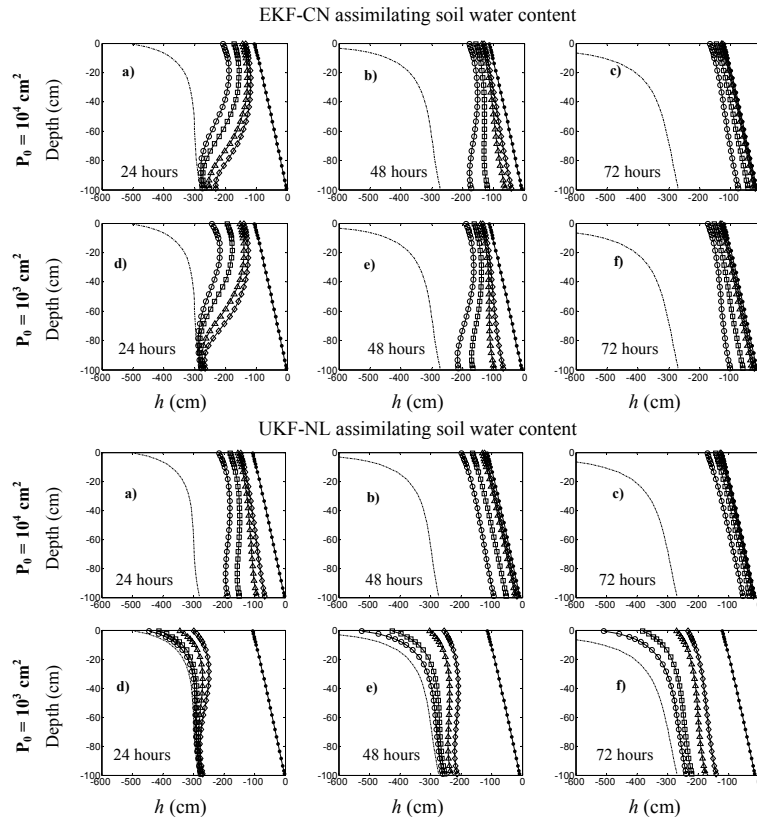


Fig. 5. Retrieved profiles from hourly assimilated observations of soil water content involving nodes within the top 0.5 cm (open circle), 1.5 cm (square), 4.5 cm (triangle) and 10.5 cm (diamond) compared with the “true” profile (closed circle) and “guess” profile (dashed line) using (a)–(f) the EKF-CN algorithm and (g)–(i) UKF-NL algorithm, with initial state covariance matrices $P_0 = 10^3 \text{ cm}^2$ and 10^4 cm^2 .

Title Page

Abstract

Introduction

Conclusions

References

Tables

Figures

◀

▶

◀

▶

Back

Close

Full Screen / Esc

Printer-friendly Version

Interactive Discussion

Part 1: Retrieving state profiles with linear and nonlinear numerical schemes

G. B. Chirico et al.

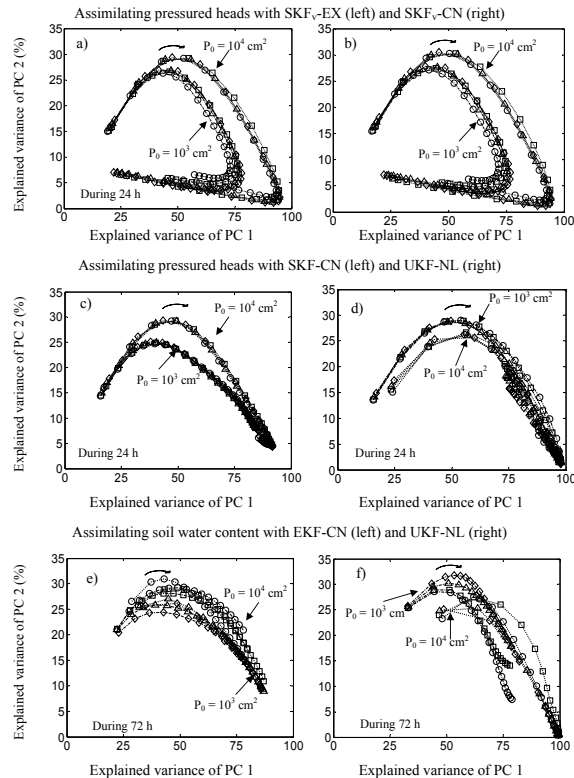


Fig. 6. Explained variance by the first (PC 1) and second (PC 2) principal components of the state covariance by assimilating hourly pressure heads with **(a)** SKF_v-EX, **(b)** SKF_v-CN, **(c)** SKF-CN, **(d)** UKF-NL within the first 24 h; and also by assimilating hourly soil water content with **(e)** EKF-CN, **(d)** UKF-NL within the first 72 h. Observation depths of 0.5 cm (open circle), 1.5 cm (square), 4.5 cm (triangle) and 10.5 cm (diamond) and initial state covariance matrices $P_0 = 10^3 \text{ cm}^2$ and 10^4 cm^2 . Time evolves according to the direction indicated by the curved arrow.